2025, 10(3)

e-ISSN: 2468-4376

https://www.jisem-journal.com/

Research Article

Advancements in Grid-Connected Solar Photovoltaic Systems: Control and Optimization with Modified SEPIC-Luo Converter

D. Thivya Prasad^{1*}, R. Anandha Kumar², P. Balamurugan³

- ^{1*}Research Scholar, Department of Electrical and Electronics Engineering, Faculty of Engineering and Technology, Annamalai University, Tamil Nadu, India. dthivyaprasad45@gmail.com
- ²Assistant Professor, Department of Electrical and Electronics Engineering, Faculty of Engineering and Technology, Annamalai University,
 Tamil Nadu, India. anand_r1979@yahoo.com
- ³Professor, Department of Electrical and Electronics Engineering, Mount Zion College of Engineering and Technology, Tamil Nadu, India. balapv@yahoo.com

*Corresponding Author: D. Thivya Prasad

- *Research Scholar Department of Electrical and Electronics Engineering, Faculty of Engineering and Technology, Annamalai University,
 Tamil Nadu, India. Email: dthivyaprasad45@gmail.com
- Citation: D. Thivya Prasad, et al. (2025), Advancements in Grid-Connected Solar Photovoltaic Systems: Control and Optimization with Modified SEPIC-Luo Converter, Journal of Information Systems Engineering and Management, 10(3)

ARTICLE INFO

ABSTRACT

Received: 18 Dec 2024

Revised: 10 Feb 2025

Accepted: 28 Feb 2025

The growing global need for energy has spurred the widespread adoption of grid-connected Solar Photovoltaic (SPV) systems. These systems harness the advantages of photovoltaic power generation, such as environmental sustainability, low maintenance requirements and noise-free operation, positioning them as a prominent Renewable Energy Source (RES). This conceptual framework emphases on demonstrating and control design of a PV grid-tied system, integrating a Modified Single-Ended Primary Inductance (SEPIC) - Luo Converter. The central objectives of this work are to investigate the behavior of solar PV systems and to develop an efficient grid-connected solar power solution. To achieve these objectives, a Maximum Power Point Tracking (MPPT) circuit is designed, leveraging Red deer algorithm optimized Adaptive Neuro-Fuzzy Inference System (ANFIS). This innovative approach ensures the continuous optimization of power extraction from solar PV modules. The DC voltage generated by the PV system is subsequently directed to a Single-Phase Voltage Source Inverter (14VSI) for conversion into AC voltage. The resulting AC voltage is then made available for various applications within the grid. Based on the simulation results, the algorithm efficiency is of 98.8% and the converter efficiency is found to be 98.92%. The MPPT efficiency is of 98.61%, which gives better optimization when compared to that of other algorithms. This framework encapsulates the advancements in SPV systems, offering a sustainable energy solution that aligns with the growing demand for clean and efficient power generation.

Keywords: PV System, Modified SEPIC-Luo, Red Deer Optimized- ANFIS MPPT Controller, PI Controller, 1ϕ VSI, 1ϕ Grid

1. INTRODUCTION

For environmental concerns and the advancement of a sustainable society, future power systems will include a significant penetration of solar power, wind power, fuel cell and small/micro-hydro power systems. Energy supply are not only linked to global warming but also to environmental concerns. The trend is to increase renewable energy while decreasing the use of fossil fuels and coal. Some potential solutions for mitigating these effects have emerged, including energy conservation through greater energy efficiency, a reduction in fossil fuel use, and an increase in ecologically friendly energy suppliers. Recently, one of the key difficulties for engineers and scientists has been the generation of energy from clean, efficient and ecologically acceptable sources. Among numerous RESs, PV energy conversion system is most preferred option due to its accessibility, ease of installation, environmental friendliness, and low cost [1] [2]. PV in power systems is defined as a stand-alone or grid-connected application as a harmless and clean source of solar energy. [3]

2025, 10(3)

e-ISSN: 2468-4376

https://www.jisem-journal.com/

Research Article

Even though PV panels are inexpensive, MPPT methods are still widely used to manage power electronic converters. The transformation ability of PV modules is limited due to nonlinear voltage/current properties. MPPTs are acute components for safeguarding superior PV energy generation in tracking a global power point [4]. Typically, efficacy of a PV system is low. As a result, a number of MPPT approaches are used to improve efficiency. Maximum power is extracted from a PV system by employing these strategies. These techniques detect the panel current or voltage, or both, at MPP and measure the parameters required to run the system. Several MPPT approaches have been developed throughout the years, like Hill Climbing (HC) [5] [6], Perturb & Observation (P&O) [7] [8], Fuzzy Logic [9] [10], ANFIS [11] [12]. However, these approaches display substantial power fluctuations around MPP and a delayed settling time in reaction to step changes. However, these approaches struggle adapting to changes in solar irradiance or temperature and the model's intricacy also pose difficulties in real-time implementation [13] [14]. Hence, to overcome these issues optimization technique has been introduced [15]. To track the optimal power, a novel ANFIS based MPPT controller with Red deer optimization has been proposed in the study.

A DC-DC converter is required for avoiding too many series-connected PV panels and achieve MPPT [16]. They are often regarded as the finest option for controlling, protecting and boosting the voltage level and efficiency of RES [17]. To advance the operation of DC-DC converters, a novel SEPIC- Luo converter have been proposed. A high-voltage DC link is formed by connecting the rectifier's DC output which is then is passed to 1¢ VSI [18] for AC voltage conversion. By controlling voltage on the grid side using a PI [19] controller, PV systems operate better in fluctuating irradiance conditions and provide stable voltage for grid applications.

In this research, novel ANFIS MPPT in PV systems is used to enhance the scheme's ability to abstract the MPP from solar panels, and adjust to shifting weather patterns. The system's performance and flexibility have been enhanced by the implementation of a Red Deer Algorithm for optimisation. A Modified SEPIC-Luo converter has been proposed which helps to reduce input and output voltage ripples, contributing to improved power quality and stability in the grid-connected system. To assure better power quality, an LC filter is employed by improving current and voltage waveforms. A single phase inverter topology has been implemented to convert the DC input from PV cell to AC output.

2. PROPOSED SYSTEM

The use of electrical energy has been increased substantially because of the tremendous rise in global population. This resulted in the installation of a PV system. This proposed scheme (Figure 1) employs a revolutionary Red Deer Optimized ANFIS topology with a combined SEPIC-Luo converter for a PV tied grid system. The power obtained from PV side is fed into the grid via the DC link. A single phase VSI was utilized to provide grid power by converting DC voltage from PV to AC voltage. It is required to optimize the system's power quality performance by using PI controller. A technique like this seeks to diminish DC link input voltage fluctuation, eliminate harmonics, steady output current, voltage, frequency and power flow in the grid side.

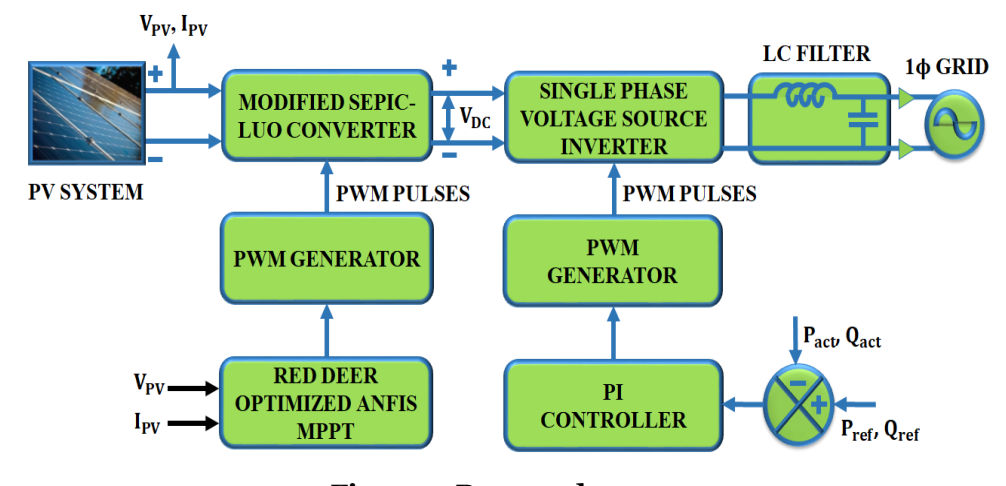


Figure 1. Proposed system

2025, 10(3)

e-ISSN: 2468-4376

https://www.jisem-journal.com/

Research Article

2.1. Modelling of PV

Due to its low voltage, PV cells are typically not controlled separately. As a result, cells are generally connected in series (Figure 2) to generate the required module output voltage. The PV module is made up of number of interconnected cells housed in a frame. A PV array is a structure that consists of a number of PV modules installed on the same plane with suitable electrical connections to produce the needed electrical power for a specific application. PV module connections in series and parallel are comparable to battery connections and are governed by Kirchhoff's lows.

The parameters of PV module are same as those of a PV cell, except that the voltage limit must be distributed by the amount of series connected cells. The PV output current equation I_{pv} is given as follows:

$$I_{pv} = I_{ph} - I_0 \left\{ exp \left[\frac{V_{pv} + I_{pv}R_s}{mV_t} \right] - 1 \right\} - \frac{V_{pv} + I_{pv}R_s}{R_{sh}}$$
 (1)

Where I_{ph} denotes photo generated current, I_0 refers PV saturation current, V_{pv} represents PV output voltage, R_s is the shunt resistance, R_{sh} denotes shunt resistance, m indicates diode ideality factor and V_t represents thermal voltage $\left(V_t = \frac{kT}{a}\right)$

 $T \rightarrow$ Temperature of the cell

 $q \rightarrow \text{Electronic charge}(1.6 * 10^{-19}C)$

 $k \rightarrow \text{Boltzmann constant } (1.38 * 10^{-23} J/K)$

The voltage equation is given by,

$$V_{pv} = N\lambda \ln \left(\frac{I_{sc} + I_{pv} + MI_0}{MI_0} \right) - \frac{N}{M} R_s I_{pv}$$
 (2)

Where N, M are the strings linked in series and parallel respectively, I_{sc} denotes short circuit current and λ is the material co-efficient.

The power generated from PV is intended as shown below,

$$P = V_{pv} * I_{pv} \tag{3}$$

In-order to regulate voltage levels, and facilitating seamless integration with the electrical grid, SEPIC Luo converters are used by enhancing the overall performance and reliability of PV systems.

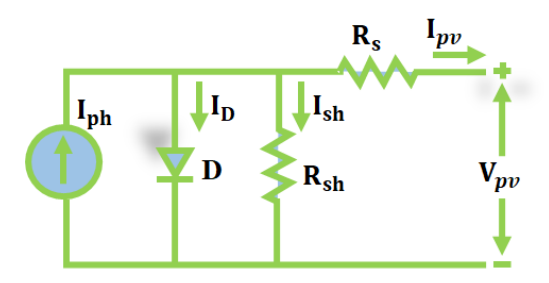


Figure 2. Modelling of PV

2.2. Modified SEPIC-Luo Converter modelling

The modified SEPIC-Luo converter, which raises the voltage on the PV side, is shown in Figure 3. The two modes of operation of converter has been shown below. For the theoretical study, all capacitors are considered voltage sources, while semiconductors are considered ideals.

2025, 10(3)

e-ISSN: 2468-4376

https://www.jisem-journal.com/

Research Article

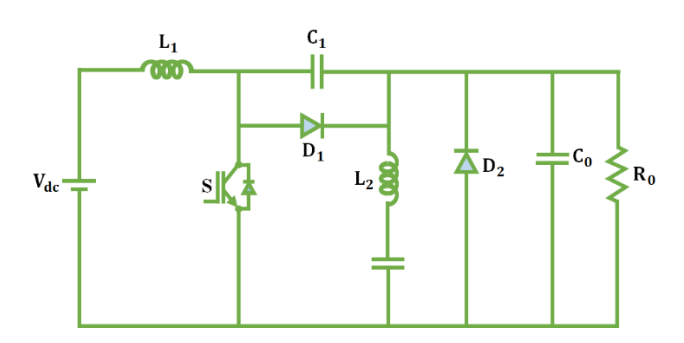


Figure 3. Modified SEPIC-Luo Converter

Mode $1[t_0 - t_1]$ (Figure 4) - At time t_0 , switch S is activated, and the diodes D_1 and D_2 are choked, while the inductors L_1 and L_2 store energy. The input voltage is applied to inductor L_1 and $V_{C_2} - V_{C_1}$ voltage is applied to inductor L_2 . The V_{C_2} voltage exceeds the V_{C_1} voltage.

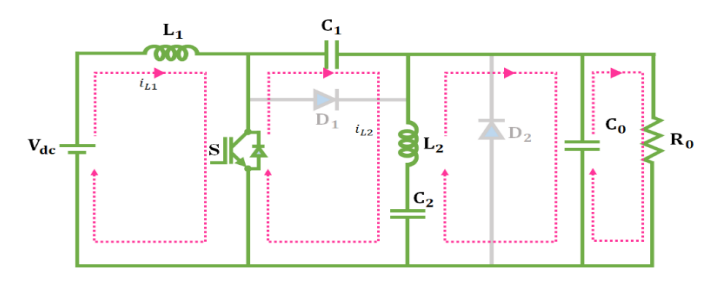


Figure 4. Switch on mode

Mode 2 $[t_1-t_2]$ (Figure 5) - At time t_1 , switch S is made off, and the energy placed in input inductor L_1 is conducted to output via C_1 capacitor and output diode D_2 , as well as to the C_2 capacitor via the diode D_1 . As a result, the switch voltage equals the C_2 capacitor voltage. The diode D_1 transfers the energy kept in inductor L_2 to the output.

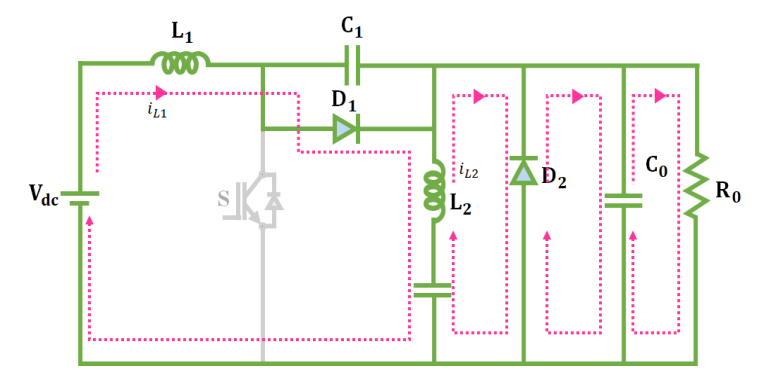


Figure 5. Switch off mode

The basic theoretical waveforms used in hard switching commutation are shown in Figure 6.

2025, 10(3)

e-ISSN: 2468-4376

https://www.jisem-journal.com/

Research Article

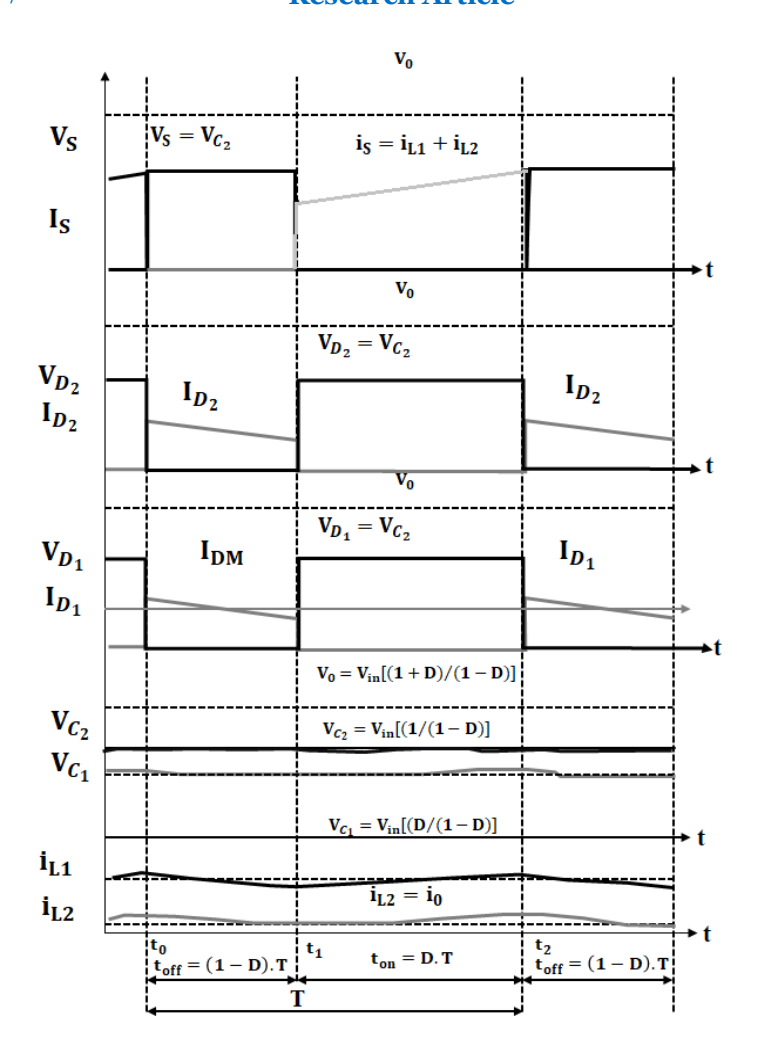


Figure 6. Theoretical waveforms of the proposed converter

The maximum voltage across all diodes and power switch is equivalent to voltage across the C_2 capacitor. The total voltage of the capacitors C_1 and C_2 is equal to output voltage. The input current is equal to mean L_1 inductor current, while output current is equal to mean L_2 inductor current.

The static gain of the proposed converter is calculated by ignoring average inductor voltage at steady-state, as shown in (4). Equation (5) calculates C_2 capacitor voltage, which is the same as output voltage of traditional converters. The V_{C_2} voltage is equivalent to the maximum switch voltage. As a result, the switch voltage is less than converter output voltage.

$$\frac{V_0}{V_i} = \frac{1+D}{1-D} \tag{4}$$

The voltage through C_1 capacitor is given by (5),

$$\frac{V_{C_1}}{V_i} = \frac{D}{1 - D} \tag{5}$$

The voltage across C_2 is given by,

$$\frac{V_{C_2}}{V_i} = \frac{1}{1 - D} \tag{6}$$

A controller in PV system enhances efficiency through advanced algorithms and real-time adjustments. An ANFIS based MPPT has been used that ensures the system to operate at its peak performance.

2.3. Modelling of ANFIS controller

2025, 10(3)

e-ISSN: 2468-4376

https://www.jisem-journal.com/

Research Article

The ANFIS design depicted in Figure 7 is composed of 5 layers, with the output of each layer designated by L_l , i where l and i denotes layer number and neuron number respectively.

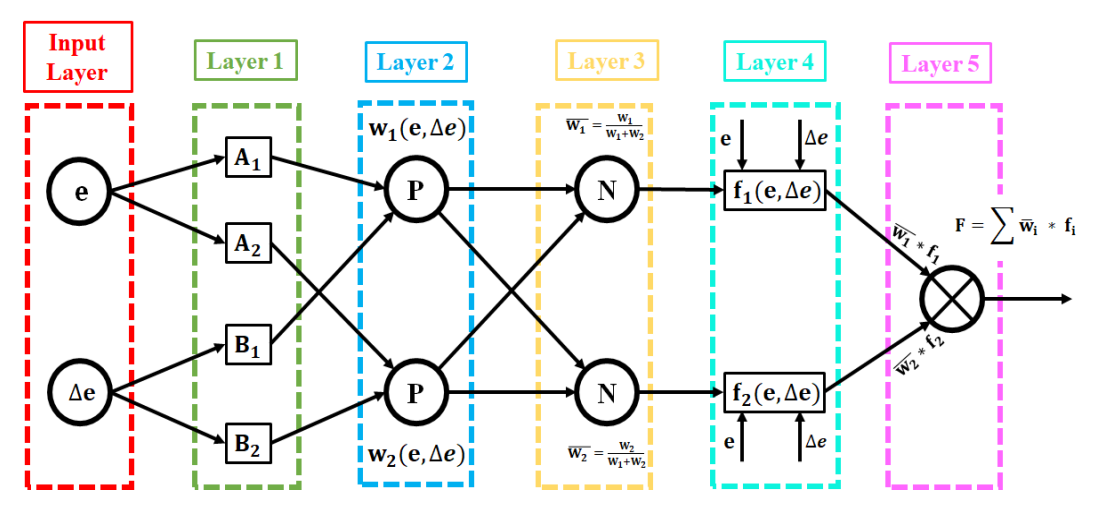


Figure 7. ANFIS architecture

The following is a full explanation of each layer:

Layer 1:

This layer downs the non-linear input using semantic variables such as small, medium, and huge and the node is referred to as an adaptive node. The equation of each node is given as follows

$$L_{1,i} = \mu A_i(e)$$

$$L_{1,i} = \mu B_i(\Delta e)$$
where $i=1,2,.....j$ (4)

Here e and Δe represent deviation and change in deviation respectively, $A_i(e)$ and $B_i(\Delta e)$ are membership functions that calculate the provided data. The membership functions are assigned to each node using the Gaussian membership function, given as follows:

$$\mu A_i(x) = exp \left[\frac{-1}{2} \left(\frac{x - c_{ij}}{\sigma_{ij}} \right)^2 \right]$$
 (5)

where c_{ij} is the mean and σ_{ij} is its variance of the j^{th} function.

Layer 2:

This layer finds the strength for each standard based on the information associated with that standard. This layer's node function is denoted as follows,

$$L_{2,i} = \mu A_i(e) * \mu B_i(\Delta e), \quad \text{where } i = 1,2$$
 (6)

Layer 3:

The normalization process is done by the nodes in this layer. The following is the node function of this layer:

$$L_{3,1} = \overline{w}_2 = \frac{w_1}{w_1 + w_2} \tag{7}$$

$$L_{3,2} = \overline{w}_2 = \frac{w_2}{w_1 + w_2} \tag{8}$$

Layer 4:

This node's function of this layer is given as follows:

2025, 10(3)

e-ISSN: 2468-4376

https://www.jisem-journal.com/

Research Article

$$L_{4,1} = \overline{w_1} f_1 = \overline{w}_1 (p_1 e + q_1 \Delta e + r_1)$$
 (9)

$$L_{4,2} = \overline{w}_2 f_2 = \overline{w}_2 (p_2 e + q_2 \Delta e + r_2)$$
 (10)

where \overline{w}_i denotes the firing strength normalized. The linear parameters (p_i, q_i, r_i) shown in equation (9, 10) are changed by the ANFIS training process.

Layer 5:

The over-all outcome of the last layer is the total of all incoming signals. This layer is known as output layer, and it has a single node, which is given as a circle node with the following node function:

$$L_{5,1} = \frac{\sum_{i=1}^{2} w_i f_i}{\sum_{i=1}^{2} w_i} \tag{11}$$

To enhance the different parameters of the ANFIS controller, Red Deer optimization algorithm has been implemented.

2.4. Red Deer Optimization Algorithm

The projected RDA flowchart is illustrated in Figure 8.

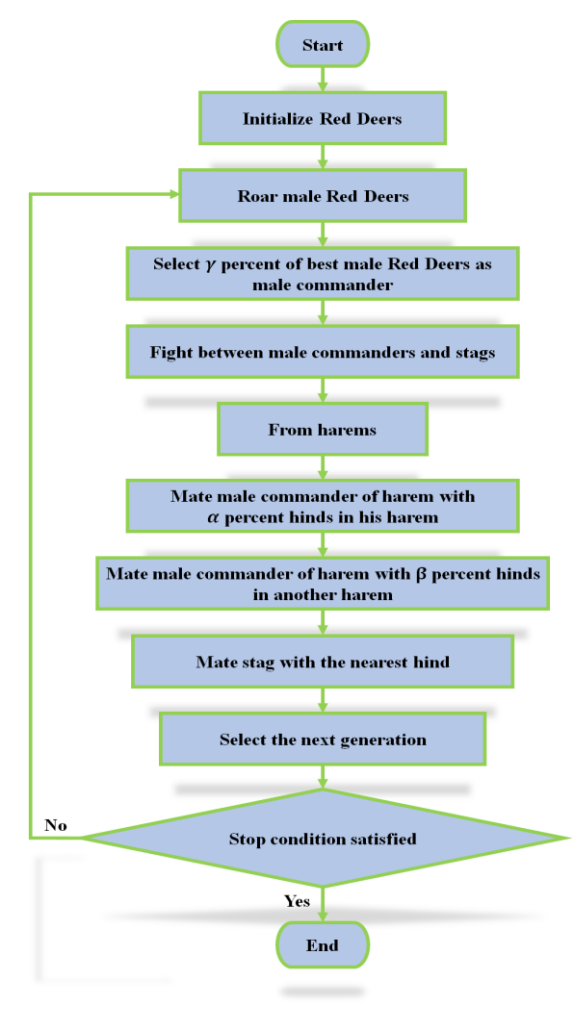


Figure 8. Red Deer Optimized controller

2.4.1. Generating Red Deers

This approach seeks to find the best answer for the issue's variable. An array known as "chromosome" in GA language which consists of certain values is made and it is denoted as "Red Deer" in this context. As an outcome,

2025, 10(3)

e-ISSN: 2468-4376

https://www.jisem-journal.com/

Research Article

Red Deer is the response's correspondingly. It is $1 * N_{var}$ array in N_{var} dimensional optimization problem. This array is defined as follows:

$$Red\ Deer = [X_1, X_2, X_3, ..., X_{var}]$$
 (12)

The value of function is given as:

$$Value = f(Red Deer) = f(X_1 X_2 X_3 \dots, X_{N_{max}})$$
(13)

To begin optimization procedure, we create a population size N_{pop} . We choose the greatest Red Deers for N_{male} and the remainder for N_{hind} .

2.4.2. Roar Male red deers

The male Red Deer roars to enhance their grace. It denotes that if male Red Deers outperform previous ones in terms of independent functions, and they swap them. So that, every male Red Deer is made to switch positions. Male Red Deer attract females by roaring.

2.4.3 Select y percent of best male Red Deers as male commanders

Male Red Deer varies greatly from one another. Some of them had greater success than others. Males are generally not as suited to nature; some even steal harems. We consider it into two types: male commanders and stags. Hence,

$$N.male.Com = round\{\gamma.N_{male}\}\$$
 (14)

Where *N. male. Com* is the no. of males grabbing the harems.

The no. of stags is calculated as follows:

$$N. stag = N_{male} - N. male. Com$$
 (15)

Where N. stag is no. of stags in male population.

2.4.4. Fight between male commanders and stags

The men battle stags for each commander at random and select them if independent function is superior to the previously stated after a combat.

2.4.5. Harems

This phase involves making harems. The harem refers to a group of hinds that have been enslaved by a male ruler.

$$V_n = v_n - \max\{v_i\} \tag{16}$$

Where v_n is nth male commander's value and V_n is its normalized value.

$$P_n = \left| \frac{V_n}{\sum_{i=1}^{N.male.Com} V_i} \right| \tag{17}$$

 P_n denotes standardised power of each male commander

From an alternative angle, a man's typical strength is the amount of hindrance that he ought to have. At that point, a harem's hind population will be:

$$N.harem_n = round\{P_n.N_{hind}\}$$
(18)

Where N.harem is the no. of hinds in n^{th} harem and N_{hind} denotes total no. of hinds. We choose one of the hinds at chance and give it to each male commander to split them. These hinds, together with male, will form the n^{th} harem.

2.4.6. Mate male commander of harem with a percent hinds in his harem

The mating action begins at stage E. In GA, we have a "crossover" model for this fact. A harem's number of hinds mating with their male leader will be proportional to α :

2025, 10(3)

e-ISSN: 2468-4376

https://www.jisem-journal.com/

Research Article

$$N.harem_n^{mate} = \{round\alpha. N.harem_n\}$$
 (19)

Where *N. harem*^{mate}_n denotes no. of hinds in the n^{th} harem. We pick *N. harem*^{mate}_n of the *N. harem* at random.

2.4.7. Mate male commander of harem with β percent hinds in another harem

Each harem has a percentage of hinds that can mate with the male commander for each harem. The number of hinds mating with one male Red Deer in a harem is given as,

$$N.harem_n^{mate} = round\{\beta.N.harem_n\}$$
 (20)

2.4.8. Mate stag with the nearest hind

Each stag is mating with the closest hind at this stage. The distance in a J-dimension between a male Red Deer and every hind is computed as follows in order to determine which hind is the closest:

$$d_i = \left(\sum_{j \in J} \left(stag_j - hind_j^i\right)^2\right)^{1/2} \tag{21}$$

2.4.9. Select the next generation

The next group of male Red Deer was determined to be the best fit, and hinds were selected for the next group by a tournament or any other evolutionary mechanism that used fitness-based selection.

2.4.10. Convergence

The halting condition might be set by a time interval, number of iterations, or the best solution ever found.

This control algorithm facilitate seamless integration with the grid, managing the bidirectional flow of electricity and ensuring grid stability. It also enhances the overall performance of the PV system by maximizing energy yield and contributing to the reliability of grid-tied solar installations.

3. RESULTS AND DISCUSSION

The suggested scheme's performance is researched and evaluated using comprehensive simulation simulations in MATLAB Simulink. In Table 1, the parameters for the proposed system are presented.

Table 1. Parameter description

Parameter	Description	
PV		
No. of PV cells	10	
Short circuit current	8.33A	
Peak power	10Kw	
Open circuit voltage	12V	
Series connected PV cells	36	
Modified SEPIC-Luo		
L_1, L_2	4.7 μF	
C_1, C_2	1mH	
R_0	100 Ω	
C_0	2200μF	
Switching frequency	10KHz	

2025, 10(3)

e-ISSN: 2468-4376

https://www.jisem-journal.com/ Research Article

Case 1:

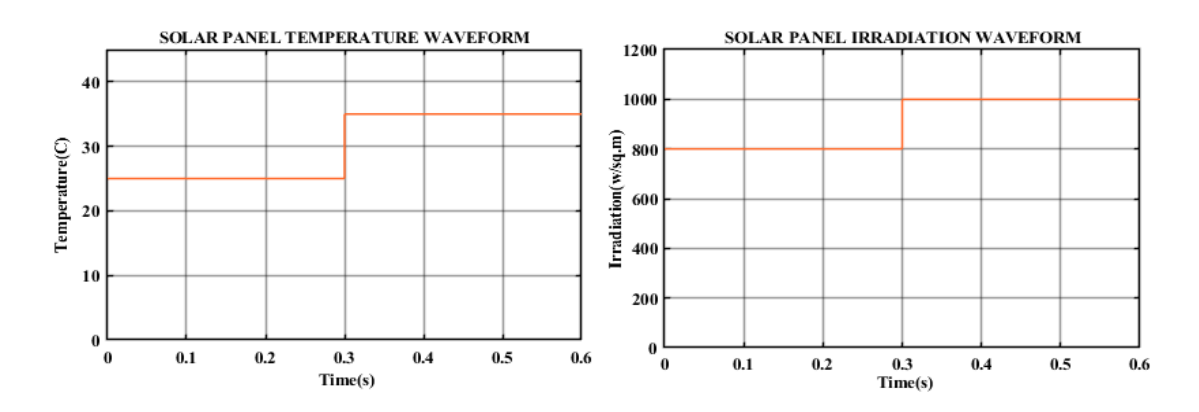


Figure 9. PV parameters for case 1 condition

A PV panel with a temperature waveform and irradiance waveform is shown in figure 9. The temperature is found to be maintained at $25^{\circ}C$ initially, rising to $35^{\circ}C$ after 0.3 seconds. Correspondingly, the irradiance of the PV is constant of 800W/sq.m, after 0.3s the value rises to 1000W/sq.m

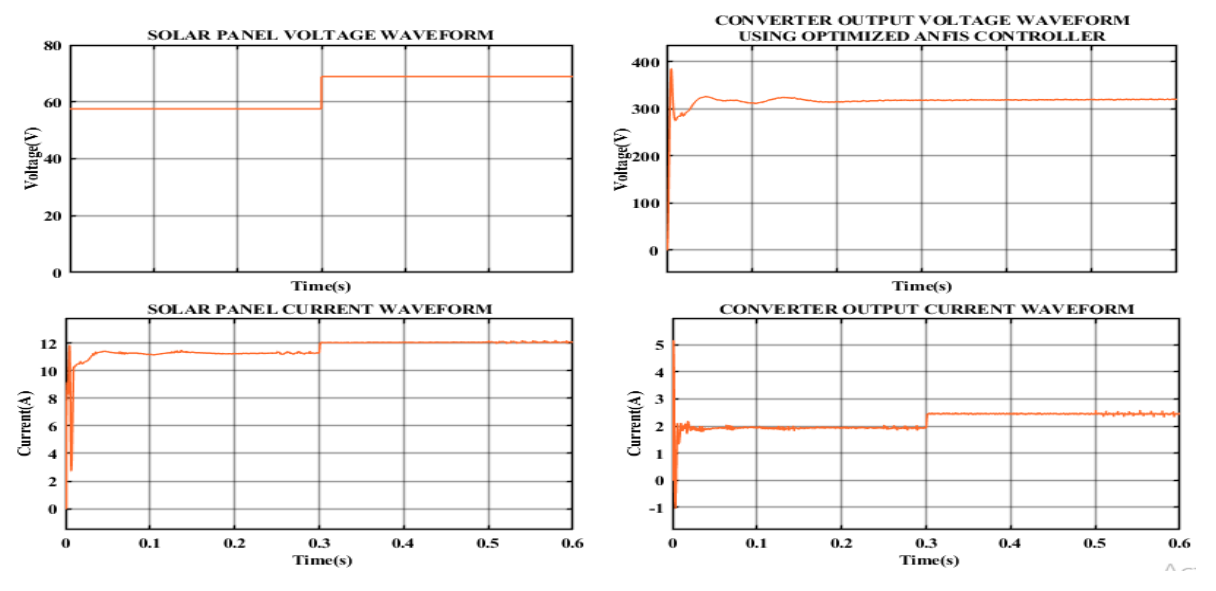


Figure 10. Voltage and current waveforms of the PV and controller

Figure 10 illustrates the voltage and current from PV and controller. Here, outputs from PV are fed as input to the converter. Initially, a constant voltage of 58V is obtained. After 0.3s, the value rises and stable voltage of 70V is obtained. At the same time, with some fluctuations initially a constant current of 11A is obtained and after 0.3 s a stable current of 12 A is obtained.

Similarly, it is noted that the output voltage of controller rises to the peak value of 390 V and then after fluctuations for some time at 0.2s a continuous voltage of 320V is attained. For the output current waveform, current value drops initially, then a constant value of 2A is maintained for some time and after 0.3s a stable current of 2.5A is obtained.

Case 2:

2025, 10(3)

e-ISSN: 2468-4376

https://www.jisem-journal.com/

Research Article

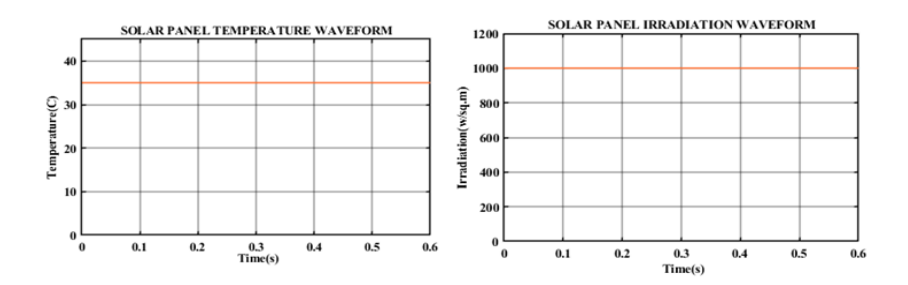


Figure 11. PV parameters for case 2 condition

Figure 11 represents temperature and irradiance waveform of PV. A stable temperature of $35^{\circ}C$ is obtained and correspondingly a stable irradiance of $1000 \, W/sq.m$ is obtained.

Figure 12 represents voltage and current output of PV and the controller. A stable voltage of 70V is obtained and after some distortions a constant current of 12A is maintained.

At the same time, voltage and current waveforms of controller shows that stable voltage of 320V is obtained after 0.2s and the current value peaks to 6A initially, later after some fluctuations it, maintains a stable current of 2.5A

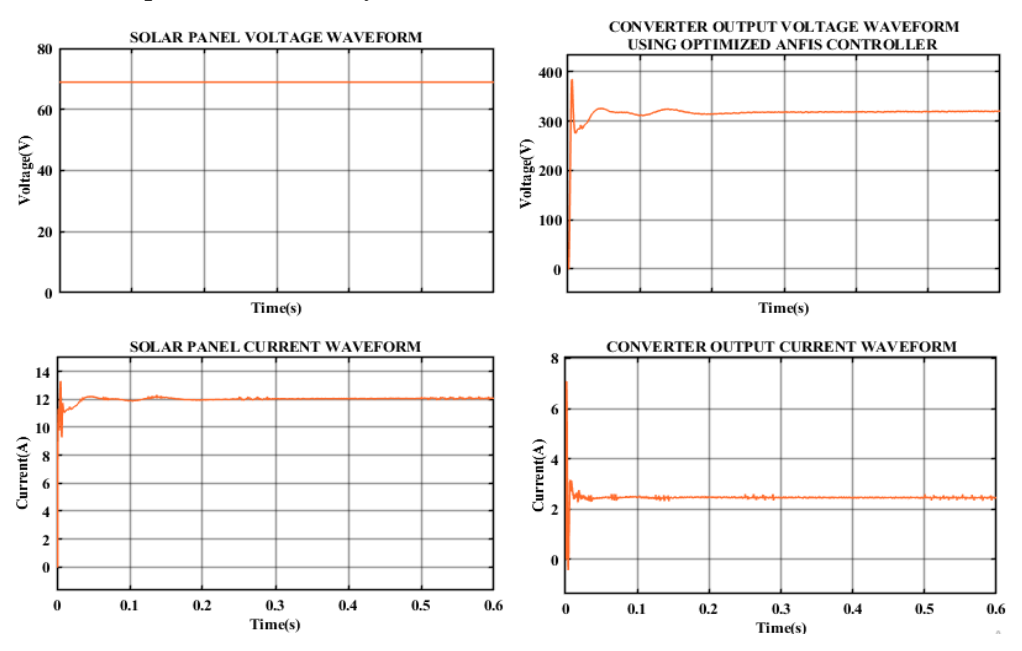


Figure 12. Voltage and current waveforms of the PV and controller

Case 3:

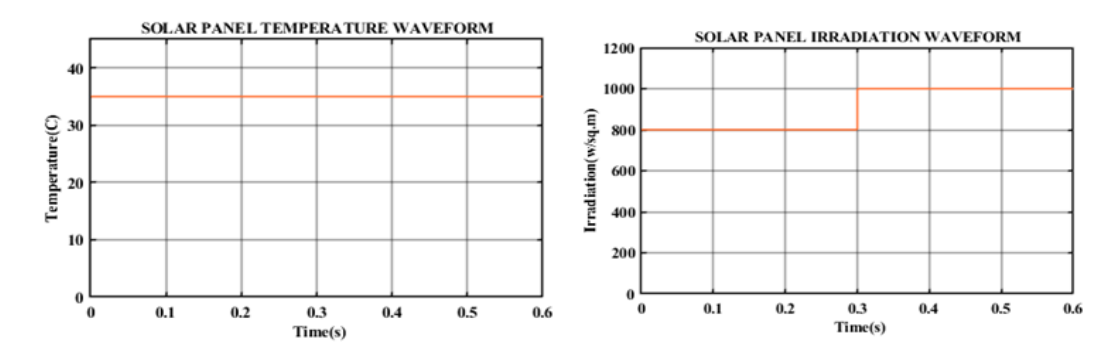


Figure 13. PV parameters under case 2 condition

2025, 10(3)

e-ISSN: 2468-4376

https://www.jisem-journal.com/

Research Article

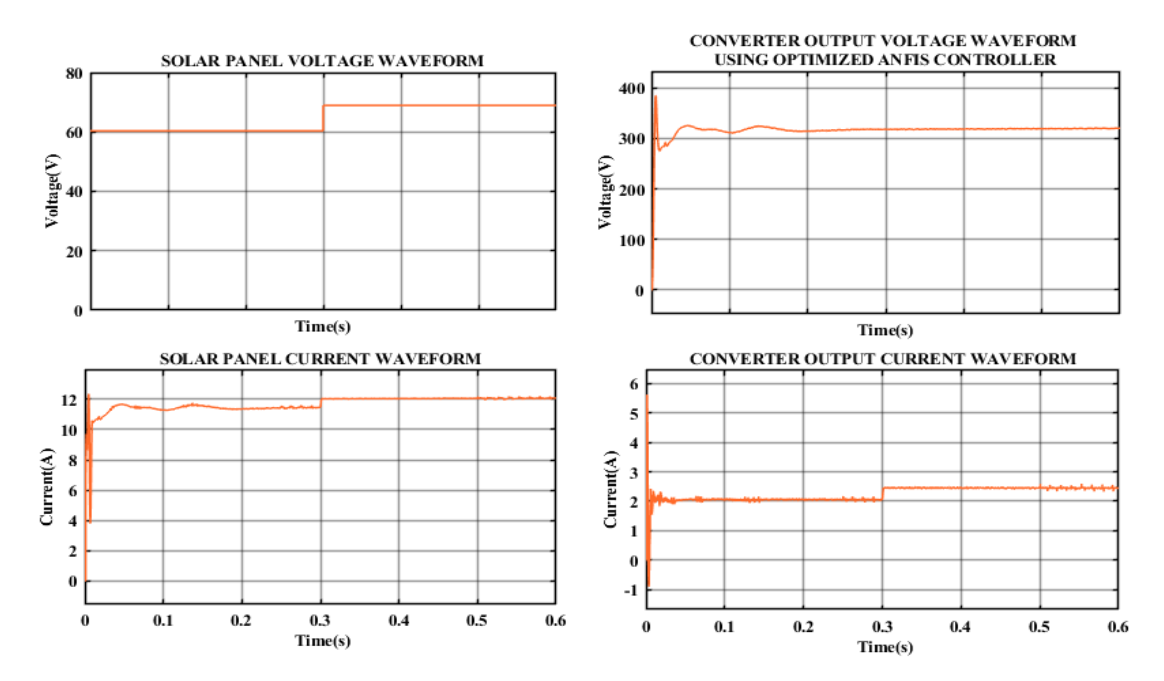


Figure 14. Voltage and current waveforms of PV and controller

Figure 13 represents temperature and irradiance waveform of the PV panel. A stable temperature of $35^{\circ}C$ is obtained and correspondingly a stable irradiance of 800 W/sq.m is obtained initially, then after 0.3s a stable value of 1000 W/sq.m is maintained.

Figure 14 shows voltage and current from PV and the controller. A steady voltage of 70V is achieved after 0.3 seconds of maintaining a constant voltage of 60V. Within 0.3 seconds, 12A is sustained at a constant rate and minor distortions appear after 0.5 seconds.

Similarly, voltage and current waveforms of controller shows that the stable voltage of 320V is obtained after 0.2s. Initially, the current value peaks to 5.5A, then it drops down and maintains a stable current of 2.5A with minor distortions.

By utilising an ANFIS controller and an optimised red deer-based MPPT method, the Modified SEPIC-Luo converter increases voltage.

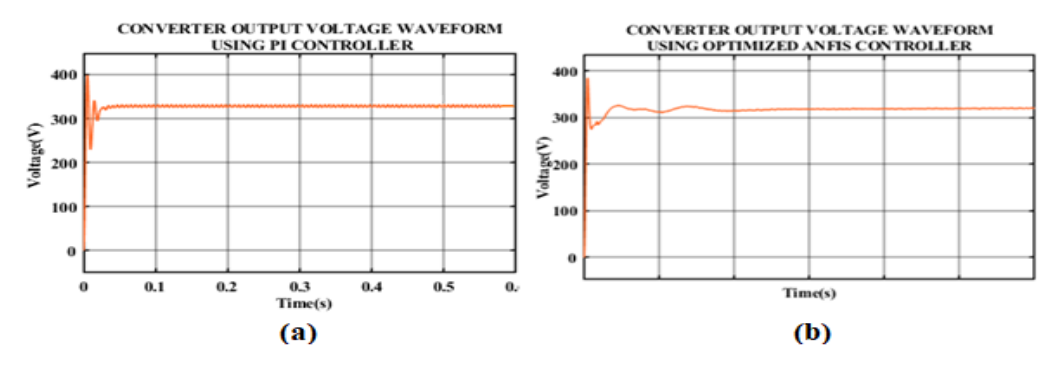


Figure 15. Output voltage waveforms of (a) PI controller and (b) Optimized ANFIS controller

The output voltage obtained using PI controller is found to be un-stabilized with fluctuations as demonstrated in Figure 15(a). Figure 15 (b) shows constant voltage of 320*V* obtained using Red Deer optimized ANFIS controller.

2025, 10(3)

e-ISSN: 2468-4376

https://www.jisem-journal.com/

Research Article

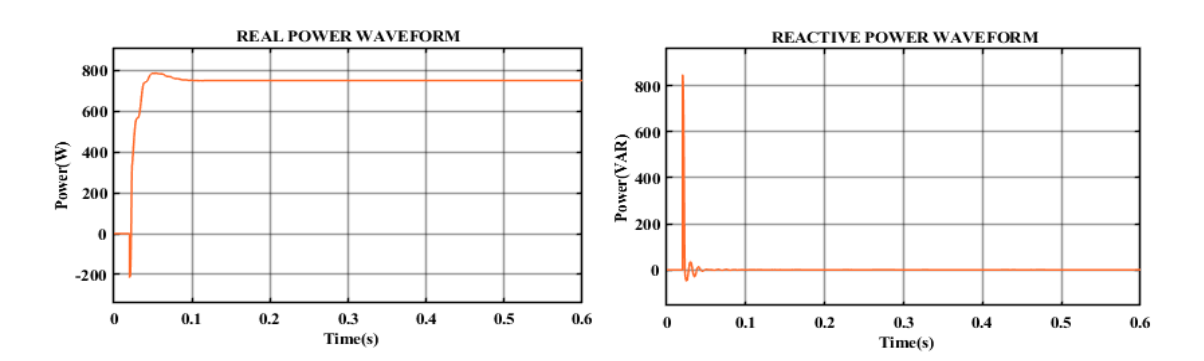


Figure 16. Waveforms of real power and reactive power of PI controller

The reactive and real power obtained with the PI controller is illustrates in Figure 16. It shows that a stable real power is obtained after 0.1s. In reactive power, the value of the power reaches a peak, then drops down to continue a constant value throughout the system.

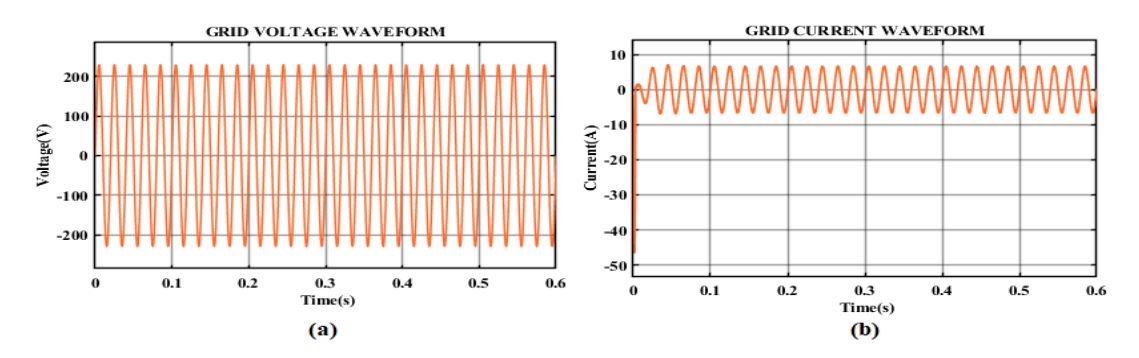


Figure 17. Grid (a) Voltage (b) Current waveforms

Figure 17 depicts the current and voltage waveforms of the grid. A constant voltage of 230V, and a constant grid current of 8A is maintained without any deviations.

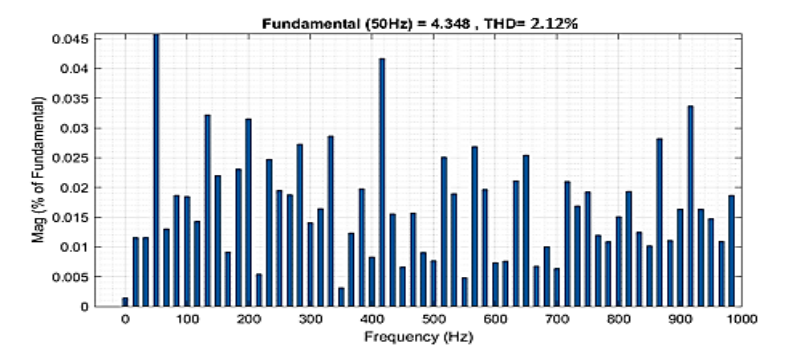


Figure 18. THD waveform of the Grid

The THD of grid is demonstrated in Figure 18. It shows that lowest THD of 2.12% is obtained using PI controller at the grid side.

Table 2. Comparison of MPPT

MPPT Technique	Efficiency %
Hill climbing	96.9 [6]
P&O	97.5 [8]

2025, 10(3)

e-ISSN: 2468-4376

https://www.jisem-journal.com/

Research Article

Fuzzy Logic	94 [10]
ANFIS-PSO	98.5 [28]
Red Deer Optimized ANFIS	98.61

Table 2 shows the efficiency of different MPPT techniques used .When compared to other techniques, the proposed MPPT obtains maximum efficiency of 98.61%

Table 3. Comparison of Converter Efficiency

Converter	Efficiency
Boost	80 [20]
Cuk	85[21]
SEPIC	88.2[22]
Luo	92.46 [23]
Luo- Boost	98.5 [27]
Modified SEPIC-Luo	98.92

Table 3 depicts the efficiency of various converters. The proposed converter achieves a maximum efficiency of 98.92% when compared to other converters.

Table 4. Comparison of Algorithm Efficiency

Optimization Algorithm	Efficiency
IGWO	98.54 [24]
LIPO	98 [25]
FFA	85.5 [26]
Red Deer Optimized ANFIS	98.8

Table 4 depicts the efficiency of different algorithms. When compared to other optimization techniques, the proposed converter obtains maximum efficiency of 98.8%.

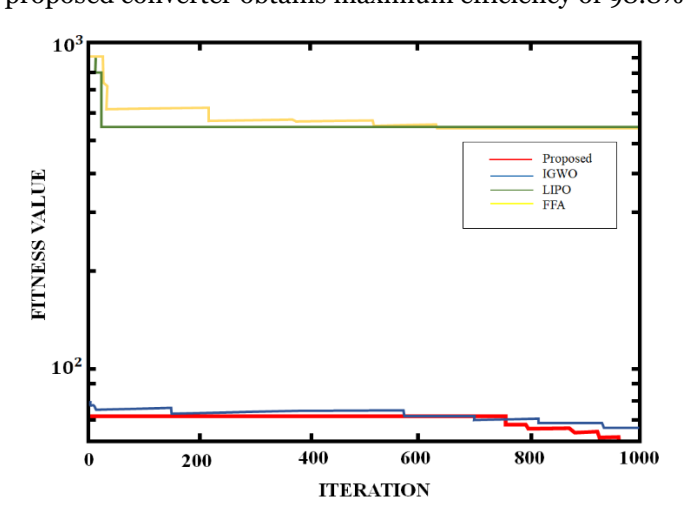


Figure 19. Convergence graph

Figure 19 represents the convergence graph of the proposed algorithm. This convergence graph serve as a tool for evaluating, and optimizing the performance of the algorithm used during the optimization process. From the figure, it is found that the proposed algorithm is of high convergence speed when compared to that of IGWO, LIPO and FFA.

2025, 10(3)

e-ISSN: 2468-4376

https://www.jisem-journal.com/

Research Article

4. CONCLUSION

As the demand for clean and sustainable energy continues to rise, the proposed work in grid-tied PV systems pave the way for more efficient and reliable PV power integration into typical energy networks. The modified SEPIC Luo converter contributes to improved energy extraction from PV modules by efficiently managing the power flow and voltage regulation. Thus, the proposed system results in a more robust and responsive grid-tied PV system. The optimization of the Red Deer Optimized ANFIS MPPT process ensures that the PV system operates at its peak efficiency, adapting to changing environmental conditions and maximizing the utilization of available PV energy. The utility of this advanced control algorithms and power management strategies contributes to enhanced grid stability. The converters enable seamless synchronization with the grid, minimizing power fluctuations and improving the system's ability to deliver consistent and reliable electricity. The proposed MPPT efficiency is of 98.61% results in the better performance of the entire system. The algorithm efficiency is of 98.8% that continuously adjust the operating point of PV to extract MPP from varying environmental circumstances. The converter efficiency is found to be 98.92%, a high efficiency, and has the ability to step up or step down the input voltage. The projected system represent a promising combination for future solar energy systems, contributing to the ongoing transition towards a greener and more sustainable energy co-ordination.

REFERENCES

- [1] M. Badoni, A. Singh, S. Pandey, and B. Singh, "Fractional-order notch filter for grid-connected solar PV system with power quality improvement," *IEEE Transactions on Industrial Electronics*, vol. 69, no. 1, pp. 429-439, 2021.
- [2] A. A. E. Tawfiq, M. O. A. El-Raouf, M. I. Mosaad, A. F. A. Gawad and M. A. E. Farahat, "Optimal Reliability Study of Grid-Connected PV Systems Using Evolutionary Computing Techniques," *in IEEE Access*, vol. 9, pp. 42125-42139, 2021.
- [3] Y. Yang, Y. Qin, S. -C. Tan and S. Y. R. Hui, "Efficient Improvement of Photovoltaic-Battery Systems in Standalone DC Microgrids Using a Local Hierarchical Control for the Battery System," in *IEEE Transactions on Power Electronics*, vol. 34, no. 11, pp. 10796-10807, Nov. 2019.
- [4] N. Priyadarshi, S. Padmanaban, J. B. Holm-Nielsen, F. Blaabjerg and M. S. Bhaskar, "An Experimental Estimation of Hybrid ANFIS-PSO-Based MPPT for PV Grid Integration Under Fluctuating Sun Irradiance," *in IEEE Systems Journal*, vol. 14, no. 1, pp. 1218-1229, March 2020.
- [5] M. Karabacak, L. M. Fernández-Ramírez, T. Kamal and S. Kamal, "A New Hill Climbing Maximum Power Tracking Control for Wind Turbines With Inertial Effect Compensation," in *IEEE Transactions on Industrial Electronics*, vol. 66, no. 11, pp. 8545-8556, Nov. 2019.
- [6] N. Shah, P. Lajevardi, K. Wojciechowski, C. Lang and B. Murmann, "An Energy Harvester Using Image Sensor Pixels With Cold Start and Over 96% MPPT Efficiency," *in IEEE Solid-State Circuits Letters*, vol. 2, no. 9, pp. 207-210, Sept. 2019.
- [7] H. Abouadane, A. Fakkar, D. Sera, A. Lashab, S. Spataru and T. Kerekes, "Multiple-Power-Sample Based P&O MPPT for Fast-Changing Irradiance Conditions for a Simple Implementation," in *IEEE Journal of Photovoltaics*, vol. 10, no. 5, pp. 1481-1488, Sept. 2020.
- [8] A. Sangwongwanich and F. Blaabjerg, "Mitigation of Interharmonics in PV Systems With Maximum Power Point Tracking Modification," *in IEEE Transactions on Power Electronics*, vol. 34, no. 9, pp. 8279-8282, Sept. 2019.
- [9] A. K. Pandey, V. Singh and S. Jain, "Maximum Power Point Tracking Algorithm Based on Fuzzy Logic Control Using P-V and I-V Characteristics for PV Array," *in IEEE Transactions on Industry Applications*, vol. 59, no. 4, pp. 4572-4583, July-Aug. 2023.
- [10] M. Y. Baramadeh, M. A. A. Abouelela, and S. M. Alghuwainem, "Maximum power point tracker controller using fuzzy logic control with battery load for photovoltaics systems," *Smart Grid and Renewable Energy*, vol. 12, no. 10, pp. 163-181, 2021.
- [11] S. A. Ibrahim, A. Nasr and M. A. Enany, "Maximum Power Point Tracking Using ANFIS for a Reconfigurable PV-Based Battery Charger Under Non-Uniform Operating Conditions," *in IEEE Access*, vol. 9, pp. 114457-114467, 2021.

2025, 10(3) e-ISSN: 2468-4376

https://www.jisem-journal.com/

Research Article

- [12] X. Tian, R. He, X. Sun, Y. Cai and Y. Xu, "An ANFIS-Based ECMS for Energy Optimization of Parallel Hybrid Electric Bus," in IEEE Transactions on Vehicular Technology, vol. 69, no. 2, pp. 1473-1483, Feb. 2020.
- [13] S. Dadfar, K. Wakil, M. Khaksar, A. Rezvani, M. R. Miveh, and M. Gandomkar, "Enhanced control strategies for a hybrid battery/photovoltaic system using FGS-PID in grid-connected mode," *International journal of hydrogen energy*, vol. 44, no. 29, pp. 14642-14660, 2019.
- [14] N. Kumar, B. Singh, B. K. Panigrashi, and L. Xu, "Leaky-least logarithmic-absolute-difference based control algorithm and learning based in C MPPT technique for grid-integrated PV system," *IEEE Transactions on Industrial Electronics*, vol. 66, no. 11, pp. 9003-9012, 2019.
- [15] I. Pervez, I. Shams, S. Mekhilef, A. Sarwar, M. Tariq and B. Alamri, "Most Valuable Player Algorithm based Maximum Power Point Tracking for a Partially Shaded PV Generation System," in *IEEE Transactions on Sustainable Energy*, vol. 12, no. 4, pp. 1876-1890, Oct. 2021.
- [16] O. Abdel-Rahim, and H. Wang, "A new high gain DC-DC converter with model-predictive-control based MPPT technique for photovoltaic systems," *CPSS Transactions on Power Electronics and Applications*, vol. 5, no. 2, pp. 191-200, 2020.
- [17] R. S. Inomoto, J. R. B. d. A. Monteiro and A. J. S. Filho, "Boost Converter Control of PV System Using Sliding Mode Control With Integrative Sliding Surface," in *IEEE Journal of Emerging and Selected Topics in Power Electronics*, vol. 10, no. 5, pp. 5522-5530, Oct. 2022.
- [18] A. A. E. Tawfiq, M. O. Abed El-Raouf, M. I. Mosaad, A. F. A. Gawad, and M. A. Elfatah Farahat, "Optimal reliability study of grid-connected PV systems using evolutionary computing techniques," *IEEE Access*, vol. 9, pp. 42125-42139, 2021.
- [19] A. Arzani, P. Arunagirinathan, and G. K. Venayagamoorthy, "Development of optimal PI controllers for a grid-Tied photovoltaic inverter," In 2015 IEEE Symp. Series on Comput. Intell., pp. 1272–1279, 2015.
- [20] F. Nejabatkhah, S. Danyali, S. H. Hosseini, M. Sabahi, and S. M. Niapour, "Modeling and control of a new three-input DC-DC boost converter for hybrid PV/FC/battery power system," *IEEE Transactions on power electronics*, vol. 27, no. 5, pp. 2309-2324, 2011.
- [21] F. Galea, M. Apap, C. S. Staines, and J. Cilia, "Design of a high efficiency wide input range isolated Cuk Dc-Dc converter for grid connected regenerative active loads", 2011.
- [22] P. Javeed, L. K. Yadav, P. Venkatesh Kumar, R. Kumar, and S. Swaroop, "SEPIC Converter for Low Power LED Applications," *In Journal of Physics: Conference Series*, vol. 1818, no. 1, p. 012220. IOP Publishing, 2021.
- [23] P. Anbarasan, M. Venmathi, M. Vijayaragavan and V. Krishnakumar, "Performance Enhancement of Grid Integrated Photovoltaic System Using Luo Converter," in *IEEE Canadian Journal of Electrical and Computer Engineering*, vol. 45, no. 3, pp. 293-302, 2022.
- [24] K. Guo, L. Cui, M. Mao, L. Zhou, and Q. Zhang, "An improved gray wolf optimizer MPPT algorithm for PV system with BFBIC converter under partial shading," *IEEE*, vol. 8, pp. 103476-103490, 2020.
- [25] W. Li, G. Zhang, T. Pan, Z. Zhang, Y. Geng, and J. Wang, "A Lipschitz optimization-based MPPT algorithm for photovoltaic system under partial shading condition," *IEEE Access*, vol. 7, pp. 126323-126333, 2019.
- [26] Y. P. Huang, M. -Y. Huang and C. -E. Ye, "A Fusion Firefly Algorithm With Simplified Propagation for Photovoltaic MPPT Under Partial Shading Conditions," in *IEEE Transactions on Sustainable Energy*, vol. 11, no. 4, pp. 2641-2652, Oct. 2020.
- [27] B. Faridpak, M. Farrokhifar, M. Nasiri, A. Alahyari, and N. Sadoogi, "Developing a super-lift luo-converter with integration of buck converters for electric vehicle applications," *CSEE Journal of Power and Energy Systems*, vol. 7, no. 4, pp. 811-820, 2020.
- [28] N. Priyadarshi, S. Padmanaban, J. Bo Holm-Nielsen, F. Blaabjerg, and M. Sagar Bhaskar, "An experimental estimation of hybrid ANFIS-PSO-based MPPT for PV grid integration under fluctuating sun irradiance," *IEEE Systems Journal*, vol. 14, no. 1 (2019): 1218-1229, 2019.